Supporting Information

Table of contents

1. Experimental Methods

Samples consisted of solutions of 1-Naphtol (1N) and 2-Napthol (2N) in dimethyl sulfoxide (DMSO), deuterated DMSO-d_6 and chloroform ($CHCl_3$). 1-Naphthol (99%) and 2-Naphthol (99%) were purchased from Aldrich and recrystallized before use. DMSO (99.7+%, Extra Dry over Molecular Sieve, AcroSeal®) was purchased from Acros Organics and DMSO-d_6 (99.50%) from Deutero. Chloroform was purchased by Aldrich. Static absorption and emission measurements were carried out on a Shimadzu UV-3600 spectrophotometer and a Shimadzu RF-5301PC spectrofluorometer, respectively.

1.1. Ultrafast fluorescence measurements

Ultrafast polychromatic fluorescence measurements in the UV (Figure 2 of the main paper) were carried out with the fluorescence up-conversion setup described in detail in ref.[S1]. In brief, the output of a Ti:Sapphire amplified laser system (4 µJ, 80fs, 150kHz) pumped an optical parametric amplifier (OPA) yielding pulses at 580 nm (65 fs, 300 nJ), which were frequency doubled in a 0.1mm-thick β-barium borate (BBO) crystal to produce the electronic excitation beam at 290 nm (20 nJ/pulse). This wavelength excites a combination of ^1L_a and ^1L_b states. The excitation beam was focused inside a flow cell where the sample was continuously circulated. The fluorescence was collected and focused into a BBO crystal where it was up-converted by mixing it with a gate beam obtained from a portion (0.5µJ/pulse) of the fundamental. The up-converted signal was dispersed by a grating on a liquid-nitrogen-cooled charge-coupled device (CCD) camera. Rotation of the BBO crystal during the accumulation time allowed for the acquisition of the full emission spectrum at each delay between excitation and gate pulses. The instrument response function (IRF) of the set-up in this configuration was 250 fs (mainly limited by the effect of group velocity mismatch in the 0.25-mm thick BBO) as measured by the FWHM of a kinetic trace of the Raman line of H_2O.

Ultrafast fluorescence anisotropy measurements (Figure 3 of the main paper) were carried out using 266 nm excitation (60 nJ/pulse) produced by tripling a portion (1/3) of the fundamental. This wavelength selectively excites the ^1L_a electronic state of both 1N and 2N with >95% selectivity, as estimated by decomposing the overall absorption spectrum into ^1L_a and ^1L_b contributions (e.g. Figure S4 and ref. [9]). The remaining 2/3 of the fundamental beam was used as a gate beam to up-convert the emission inside a BBO crystal. Anisotropy measurements were carried out in single-wavelength detection mode. This choice allowed us to use a 0.1-mm thick BBO for the upconversion, which in turn provides a substantially better IRF (140 fs) as compared to polychromatic fluorescence measurements (250 fs), where a thicker (0.25 mm) crystal was necessary to detect the signal spreading over the whole wavelength detection range. We estimate that in typical experimental conditions the fastest dynamics of anisotropy that we can reliably measure (by applying a deconvolution procedure to the data) occurs with an exponential relaxation time constant of ~40 fs. A waveplate was used to set the polarization of the excitation beam to be parallel or perpendicular to that of the gate. We obtained the anisotropy by independently measuring the emission in parallel (I_{par}) and perpendicular (I_{perp}) polarization, at the spectral position where the fluorescence band was found to peak at short delay times. The anisotropy was then calculated by the usual expression:[13]

$$r = \frac{I_{par} - I_{perp}}{I_{par} + 2I_{perp}} \qquad\qquad (1)$$

For 1N-DMSO, for the sake of comparison, we also measured the fluorescence anisotropy at two additional wavelengths falling on the right and left side of the emission band (Figure S2). All anisotropy measurements were carefully corrected for the depolarization effects induced by the parabolic mirrors collecting the fluorescence, and for the finite contrast of the wave plate. To this aim we used as benchmarks the anisotropy of a known dye and that of the Raman signal of water excited at 400 nm or at 266 nm. In all time-resolved fluorescence measurements, the concentration of the molecule in solution was chosen to absorb approximately 0.3 OD through the 0.2 mm flow cell at the excitation wavelength.

1.2 Transient infrared absorption measurements

Ultrafast IR absorption spectra were recorded using an experimental set-up described previously.[S2] Electronic excitation of 1N and 2N was achieved with pulses (3 µJ, 50 fs) generated by sum frequency mixing the fundamental of a 1 kHz amplified Ti:sapphire laser (Tsunami oscillator with Spitfire Pro regenerative and booster amplifier stages, Spectra Physics) with visible pulses generated by a noncollinear optical parametric amplifier (NOPA). The excitation wavelength was tuned to the lowest energy peak of the ^1L_b transition (325nm for 1N and 335 nm for 2N), ensuring minimal excess energy. The pump pulses were sent to a delay line and then focused onto the sample with a beam diameter of approximately 200 µm. Tunable mid-infrared pulses were generated by a double-pass OPA followed by difference frequency mixing of signal and idler. The probe and reference pulses were obtained using reflections from a ZnSe wedge, and focused onto the sample by means of an off-axis parabolic mirror (focal diameter 150 µm). The probe and reference pulses were dispersed in a polychromator ($\approx$10 cm^{-1} resolution) and spectrally resolved absorbance changes were recorded simultaneously for each shot using a liquid nitrogen cooled HgCdTe double array detector (2x31 pixels). The time resolution was determined to be 200 fs based on the cross-correlation between the UV pump and IR-probe pulses measured in a ZnSe semiconductor placed at the sample position. A peristaltic pump was used to circulate the 50 mM 1N or 2N sample through a flow cell (1 mm thick CaF$_2$ windows separated by a 50 µm thick teflon spacer), to guarantee that a new sample volume was excited for every laser shot.

Given the formation of a photoproduct sticking to the cell window which is a well-known phenomenon in aromatic systems with electron donating substituents, the sample holder was moved up and down during all time-resolved (polychromatic fluorescence, fluorescence anisotropy and transient IR) measurements. Furthermore the steady-state electronic and infrared spectra before and after the measurements were monitored to ensure that the nature of the solution did not change.

2. Theoretical calculations

All calculations were performed using the Gaussian 09 package. The geometry optimizations were carried out using DFT (for the ground state S$_0$) and TDDFT (for the ^1L_a and ^1L_b excited states) at the B3LYP/TZVP level. The absorption or emission transition dipole moments (TDMs) were computed using TDDFT at the B3LYP/TZVP level. The polarization continuum model was used to include the effects of solvation. The order of the excited states, ^1L_a and ^1L_b, in the energy ladder of 1N-DMSO, 2N-DMSO and 1N in chloroform was found to be switched with respect to the

energetic order probed by experiments. However, the distinct electronic symmetry of these states enabled us to identify unambiguously the ^1L_a and ^1L_b states.[S3]

The calculations identified four stable conformers of the 2N-DMSO complex in DMSO solution (Figure S5), with different orientations of the O-H group relative to the aromatic ring system, and of the hydrogen-bonded DMSO molecule. The populations of the four conformers when the molecule occupies each of the three electronic states (S_0, ^1L_b, ^1L_a) were estimated (Table S1, first three columns) based on the relative energetics. As for the 1N-DMSO complex in DMSO solution, the calculations predict that only three (Figure S6) out of these four isomers are appreciably populated (Table S3). Finally, the estimated populations of the cis- and trans- isomers of uncomplexed 1N in CHCl$_3$ solution are reported in Table S2.

The calculated transition dipole moment (TDM) vectors are also reported in Tables S1-S3. The TDMs of the $S_0 \rightarrow$ ^1L_a transition were calculated separately for each of the conformers based on the geometry optimized in the S_0 electronic state. For each of the three cases investigated (1N-DMSO in DMSO solution, 2N-DMSO in DMSO solution, 1N in CHCl$_3$), this procedure yields the absorption TDMs $\boldsymbol{\mu_{abs, k}}$, where k is an index running on the conformers. Similarly, the $^1L_b \rightarrow S_0$ and $^1L_a \rightarrow S_0$ conformer-dependent emission TDMs, indicated as $\boldsymbol{\mu_{b, k}}$ and $\boldsymbol{\mu_{a, k}}$ respectively, were calculated in the optimized ^1L_b (^1L_a) state geometries.

The IR spectra were computed using the Gaussian 09 package.

3. Analysis of anisotropy data

1N or 2N molecules are electronically excited to the ^1L_a state at $t=0$. At a given delay t_0, each molecule will populate one of its two excited states (^1L_a or ^1L_b), depending on the outcome of internal conversion and/or level crossing dynamics between $t = 0$ and $t = t_0$. A pure population equilibration scenario, where the nature of the original ^1L_a or ^1L_b electronic states is unchanged, is assumed. If we indicate with ρ (1-ρ) the fraction of molecules which populate the ^1L_a (^1L_b) state at $t = t_0$, the quantity ρ represents the (time-dependent) ^1L_a character of the emission. In section (3.2) we relate ρ to the experimentally measured anisotropy r. To this aim, we first estimate (3.1) the characteristic anisotropy values associated with ^1L_a and ^1L_b emission, indicated by r_A and r_B respectively: they represent the limiting values of r that one should measure in a situation in which all the molecules (initially promoted to ^1L_a at time zero) populate the ^1L_a or ^1L_b states, respectively.

3.1 Characteristic anisotropy values associated with ^1L_a and ^1L_b emissions.

Since electronic excitation at 266 nm selectively populates the ^1L_a state, a zero-order approximation would be to assume r_A=0.4 (corresponding to a zero absorption-emission angle) and r_B close to -0.2 (90° absorption-emission angle). However, r_A could deviate from 0.4 due to geometrical rearrangement and/or re-equilibration between conformers after photo-excitation, thereby altering the direction of the $^1L_a \rightarrow S_0$ TDM with respect to the $S_0 \rightarrow {}^1L_a$ TDM. In addition, unlike naphthalene, where the TDM of the two transitions are exactly perpendicular, r_B is not expected to be precisely -0.2 in the naphthols where the symmetry is broken by the OH group. For these reasons, we used TDDFT to obtain quantitative estimates of r_A and r_B to be compared with experiment.

Based on the TDMs provided by TDDFT, we can calculate r_A and r_B by doing the following conformer-averaging procedure. If a molecule is photo-excited while being in its k-th conformer configuration and emits while being in its h-th conformer configuration, its fluorescence anisotropy will equal $r_{s,kh} = 0.2\,(3\cos^2\varphi_{s,kh} - 1)$, where the index s indicates the emitting state (s=A or B), $\varphi_{s,kh}$ is the angle between the vectors $\boldsymbol{\mu}_{\mathbf{abs, k}}$ and $\boldsymbol{\mu}_{\mathbf{b, h}}$ (for ^1L_b emission) or $\boldsymbol{\mu}_{\mathbf{abs, k}}$ and $\boldsymbol{\mu}_{\mathbf{a, h}}$ (for ^1L_a emission). These vectors are reported in Tables S1-S3. Since k and h go from one to the number of isomers N, this procedure leads to enumerate N^2 situations ($k=1...N, h=1...N$) each associated to a defined value of anisotropy $r_{s,kh}$ for either of the two emission transitions. The overall conformer-averaged fluorescence anisotropy will be an average of the values $r_{s,kh}$, weighted[1] with the probabilities $p_{s,kh}$ of these (k,h) situations.

If we assume the molecules to undergo complete conformer equilibration after photo-excitation (faster than our time resolution) the values of $p_{s,kh}$ are expected to equal $f_{0,k}\,f_{s,h}$, where $f_{0,k}$ ($f_{s,h}$) are the equilibrium populations of the conformers in the ground state (in the emitting excited state). The values for $f_{0,k}$ and $f_{s,h}$ are reported in Tables S1-S3. Thus we get:

$$r_s = \sum_{k,h} p_{s,kh}\, r_{s,hk} = \sum_{k,h} f_{0,k} f_{s,h}\, r_{s,hk} = 0.2(3\sum_{k,h} f_{0,k} f_{s,h} \cos^2\varphi_{s,kh} - 1) \tag{2}$$

where we used the fact that the $p_{s,kh}$ sum up to one. Equation (2) allows the estimation of $r_s = r_A$ or r_B based on the results of TDDFT calculations. The results of this procedure are reported in Table S4. We note that r_A is always close to 0.4, i.e. TDDFT rules out strong changes of the TDM due to geometrical rearrangements. Alternatively, one can consider the other limiting situation where there is no re-equilibration at all between conformers after photoexcitation. In this case $p_{s,kh}$ will be nonzero only when $k=h$, and will equal $f_{0,k}$. The values of r_A and r_B obtained by this alternative approach are found to be very close (within 10^{-3}) to those obtained by Eq. (2).

3.2 Relation between anisotropy and the ^1L_a character of the emission

Using the limiting values r_A and r_B, we can relate the experimental anisotropy r to the amount, ρ, of ^1L_a character of the emission. The overall anisotropy of an ensemble of molecules distributed between the ^1L_a and ^1L_b electronic states will be an average of r_A and r_B weighted by the fractional emission intensities.[13] In order to express the emission intensities of the two sub-populations, we note that the fluorescence upconversion signal is proportional to the population of the emitting state (ρ and $1-\rho$ for ^1L_a and ^1L_b respectively) and to the radiative rate, which in turn is proportional to the squared magnitude $|\vec{\mu}|^2$ of the TDM (expected to be different for the ^1L_a and ^1L_b transitions). Thus, the overall anisotropy equals:

$$r = \frac{\rho|\vec{\mu}_A|^2 r_A}{\rho|\vec{\mu}_A|^2 + (1-\rho)|\vec{\mu}_B|^2} + \frac{(1-\rho)|\vec{\mu}_B|^2 r_B}{\rho|\vec{\mu}_A|^2 + (1-\rho)|\vec{\mu}_B|^2} = \frac{\rho\alpha^2 r_A + (1-\rho) r_B}{(1-\rho) + \rho\alpha^2} \tag{3}$$

---

[1] Strictly speaking, the values of $r_{s,kh}$ for a given transition (s=A or B) should be also weighted by the spontaneous emission rates (proportional to $\boldsymbol{\mu}_{\mathbf{b, h}}^2$ or $\boldsymbol{\mu}_{\mathbf{a, h}}^2$), which could be, in principle, conformer-dependent. This has, however, negligible effects because the squared magnitudes of the TDMs in Tables S1-S3 turn out to be almost conformer-independent. In contrast, a factor proportional to $\boldsymbol{\mu}^2$ must necessarily be taken into account when considering a combination of ^1L_a and ^1L_b emissions (as in Eq. 3) because the emission rates of the two electronic states are significantly different.

where $\alpha = |\vec{\mu}_A|/|\vec{\mu}_B|$ is the ratio between TDMs, and r_A, r_B are the values in Table S4. Because the squared magnitude of the TDM is also proportional to the absorption oscillator strength, we can accurately determine α from the experimental optical absorption data. This is done by decomposing the OA spectrum into ^1L_a and ^1L_b contributions, since α^2 equals the ratio of the two areas. For 2N-DMSO, where the two absorption bands are well resolved (see Figure 1), we estimate $\alpha_{2N-DMSO} = 1.75 \pm 0.05$ by direct integration. A decomposition is necessary for 1N in CHCl$_3$, as shown in Figure S4, where we find $\alpha_{1N \text{ in } CHCl3} = 1.40 \pm 0.05$. Applying the same procedure to the OA of 1N-DMSO we estimate $\alpha_{1N-DMSO} = 1.10 \pm 0.10$. The values of ρ plotted in Figure 3B were found from the experimental anisotropies of Figure 3A by inverting Eq. 3, based on the three values of α above.

It is worth noting that the slight solvent-dependence of α in 1N ($\alpha_{1N \text{ in } CHCl3} = 1.4$ vs $\alpha_{1N-DMSO} = 1.1$) we find here is actually evident by direct inspection of the OA spectra in Figure 1A, normalized to the peak at 325 nm of predominantly ^1L_b character: indeed, the area below the high-energy tail mainly due to the ^1L_a state is appreciably greater for 1N in CHCl$_3$ than in DMSO. Possible explanations of these solvent-induced changes of the relative cross sections of the two transitions are: (a) 1N forms a molecule-solvent complex only in DMSO (b) Solvent-assisted quantum mechanical state mixing between the ^1L_a and ^1L_b states (as defined in the gas phase), altering the nature and the intensity of the two transitions.

We finally discuss the fit shown in Fig. 3B of the main paper. In order to carry out a meaningful fitting procedure of these data, one may begin with assuming an exponential growth of $\rho(t)$:

$$\rho = a - b e^{-\frac{t}{\tau}} \qquad . \tag{4}$$

However, experimental data are expected to follow Eq. (4) only in the ideal case of infinitely small temporal resolution, whereas the experiment is conditioned by the finite instrumental response function (IRF) of the setup. Assuming a Gaussian IRF of full width at half maximum $\Delta = 140$ fs, it is easy to derive that the expected time dependence of $\rho(t)$ in the real experiment is the following:

$$\rho(t) = \frac{a \, erfc(t;\Delta) - b \, erfexp(t;\tau;\Delta)}{erfc(t;\Delta)} \tag{5}$$

where $erfc(t;\Delta)$ is the error function, arising from the convolution of a step function $S(t)$ with the Gaussian IRF, while $erfexp(t;\tau;\Delta)$ is the result of the convolution of the IRF with the product of $S(t)$ and the exponential decay Eq. (4). Equation (5) was used to fit the data in Fig. 3B of the main paper with three free parameters a, b, τ. From the fit we obtained a=0.42, b=0.34, τ=0.062 ps.

4. Ultrafast response of the C-O stretching mode of 1N

IR spectroscopy is a well-established method that can provide insight on the hydrogen bond strengths of a large variety of hydrogen-bonded systems.[S4-S8] Typically the hydrogen stretching oscillators are probed as they are strongly sensitive to changes in hydrogen bond geometries. It is our objective to determine the hydrogen bonding characteristics

6

of 1N in $CHCl_3$ and DMSO solvents in the electronic ground and excited states. However, given the frequency downshift and substantial broadening of the O-H stretching mode of the hydrogen bonded 1N-DMSO complex in both the ^1L_b- or ^1L_a-states, it proved impossible to reliably measure this vibration within the current experimental constraints (the same argument applies for 2N-DMSO[S9]). The hydrogen bending and wagging modes are not of local nature and are located in spectral regions made opaque by strong solvent bands. However, we identified a vibrational transition around 1276-1280 cm^{-1} in the ground-state, that exhibits a clear correlation in frequency upshift with decreasing O-H stretching frequency (Figure S3-c). DFT calculations show that for 1N in the S_0-state this vibrational transition is due to a mode with a dominant C-O stretching character (Fig. S3-a,b). As a result, we can monitor the transient IR response of this ν(C-O) mode in this spectral region to locate the solvent-dependent vibrational frequency in either ^1L_b- or ^1L_a-states. Figure S3-d shows that at a 10 ps pulse delay, the transient IR spectrum shows not only the bleach contributions due to the ν(C-O) transition of 1N in the S0-state, but also a significantly frequency-upshifted band that we tentatively assign to the ν(C-O) transition in the ^1L_b-state for 1N-CH_3CN and 1N-DMSO-d_6 complexes in C_2Cl_4, and to the ν(C-O) transition of the ^1L_a-state for 1N-DMSO-d_6 . Finding frequency upshifts of several tens of cm^{-1}as well as a larger line broadening upon electronic excitation of the hydrogen-bonded complexes of 1N, strongly suggests that the hydrogen-bond increases in strength from the ground to the excited-state, and also from the ^1L_b- (1N-DMSO complex in C_2Cl_4) to the ^1L_a-state (1N in DMSO solvent). This is in line with the traditional photoacidity ansatz as well as the larger charge transfer character of the ^1L_a-state. As visible in Fig. 2 of the main paper, these changes of the IR-active fingerprint patterns, associated to a change of the electronic state, occur within time resolution, no dynamics being observed from 200 fs up to 1.3 ns.

As a final remark we emphasize that the increase of the overall baseline in Fig. 4A can be attributed to the absorption by solvated electrons produced by photo-ionization of 1N occurring with a low quantum yield. Indeed, photo-induced ionization of naphthols, phenols (and to a greater extent their respective anions) following single photon excitation has previously been demonstrated, [S10] and solvated electrons are known to absorb throughout the mid IR. [S11]

References

[S1]: A. Cannizzo, O. Bräm, G. Zgrablic, A. Tortschanoff., A. Ajdarzadeh Oskuei, F. van Mourik, M. Chergui, *Opt. Lett* **2007**, *32*, 3555-3557.

[S2]: M. Rini, A. Kummrow, J. Dreyer, E. T. J. Nibbering, T. Elsaesser. *Faraday Discussions* **2003**, *122*, 27-40.

[S3]: M. Prémont-Schwarz, D. Xiao, V. S. Batista and E. T. J. Nibbering, J. Phys. Chem .A **2011**, *115*, 10511-10516.

[S4] A. Novak, *Struct. Bonding* (Berlin) **1974**, *18*, 177-216.

[S5] A. Laurié, F. Froment, A. Novak, *Spectrosc. Lett.* **1976**, *9*, 289-299.

[S6] W. Mikenda, *J. Mol. Struct.* **1986**, *147*, 1-15.

[S7] W. Mikenda, S. Steinböck, *J. Mol. Struct.* **1996**, *384*, 159-163.

[S8] E. Libowitzky, *Monats. Chem.* **1999**, *130*, 1047-1059.

[S9] M. Prémont-Schwarz, D. Xiao, V. S. Batista and E. T. J. Nibbering, in: *Ultrafast Phenomena XVIII*, M. Chergui, A. J. Taylor, S. Cundiff, K. Yamanouchi and R. de Vivie-Riedle, eds., *in press.*

[S10]: N. Getoff, Radiation *Physics and Chemistry* **1989**, *34*, 711-719; J. C. Mialocq, J. Sutton, P. Goujon, Journal *of Chemical Physics* **1980**, *72*, 6338-6345.

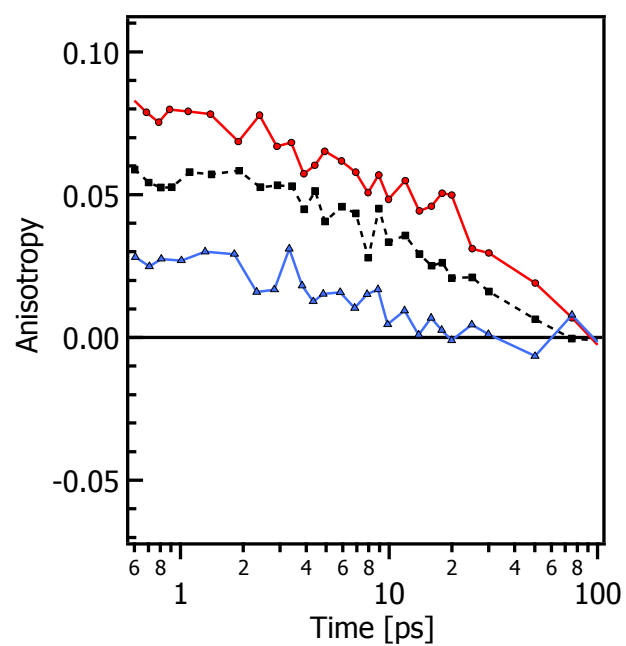[S11]: A: Thaller, R. Laenen, A. Laubereau, *Chem. Phys. Lett.* **2004**, *398*, 459-465.

Figure S1: Fluorescence anisotropy measured at long times in 1N-DMSO (continuous red line), 1N in CHCl$_3$ (continuous blue line) and 2N in DMSO (black dashed line). The anisotropy decreases to zero on a time scale of a few tens of ps due to rotational diffusion.
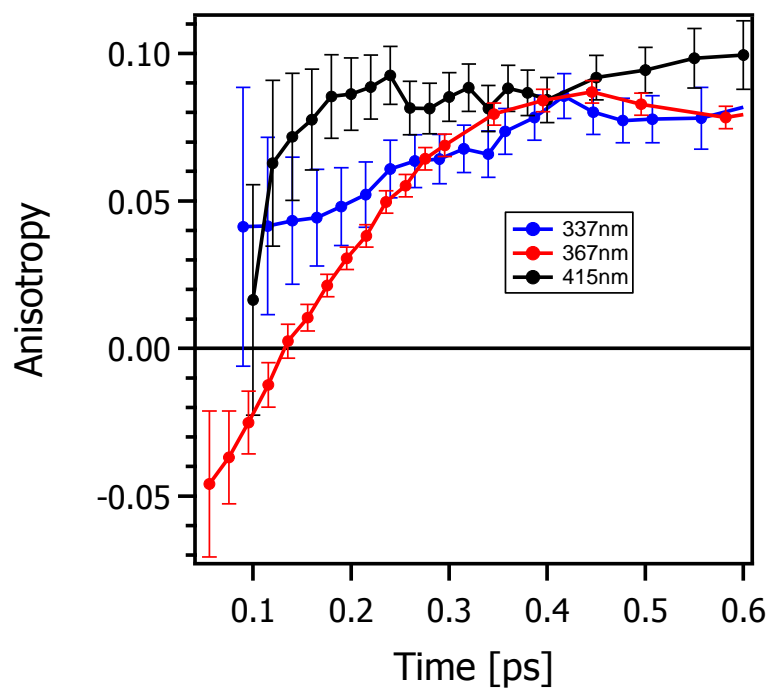
Figure S2: Fluorescence anisotropy measured at three emission wavelengths in 1N-DMSO after excitation at 266 nm. Data at 367 nm are the same as in Figure 3A in the main paper. At short times (t < 0.1 ps), reliable measurements of the anisotropy on the left (337 nm) and right (415 nm) wing of the emission band were hindered by the very low intensity of the fluorescence upconversion signal.
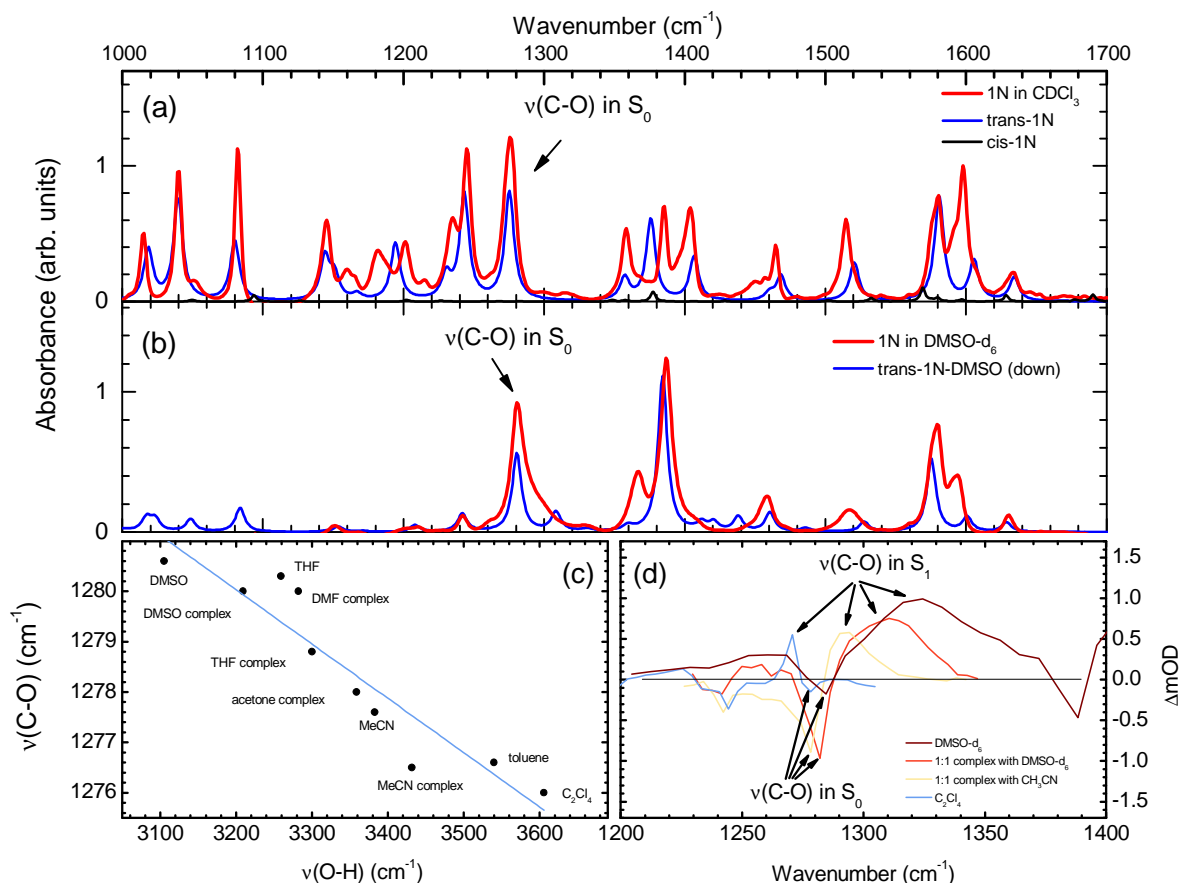
Fig S3: Steady-state IR spectra of the fingerprint region of 1N in CDCl$_3$ (a) and in DMSO-d$_6$ (b) are compared with the relative contributions of different rotamers as determined by DFT calculations. The ν(C-O) and ν(O-H) frequencies exhibit a clear correlation (c). Transient IR spectra show the pronounced solvent dependence of the ν(C-O) mode of 1N in the ^1L_b- or ^1L_a-states, whose frequency is upshifted as compared with the ν(C-O) mode of 1N in the S_0-state.
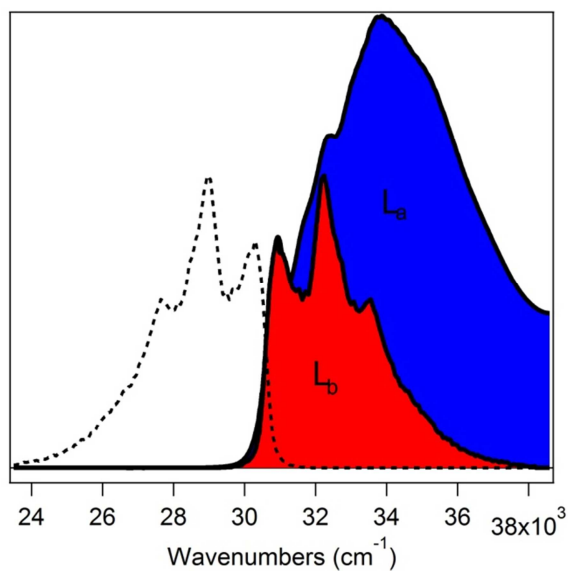
Figure S4: Decomposition of the absorption band of 1N in $CHCl_3$ in ^1L_a (blue shaded area) and ^1L_b (red shaded area) contributions, the latter being estimated by applying a mirror-symmetry operation to the almost pure ^1L_b emission (dashed black line) measured in $CHCl_3$. As mentioned in (3.2), from the ratio between the two areas we calculated the parameter $\alpha_{1N\ in\ CHCl_3}$=1.40 ± 0.05, i.e. the ratio between the magnitudes of the TDMs of the two transitions. The same decomposition procedure was carried out for the absorption of 1N in DMSO, for which we estimate $\alpha_{1N\text{-}DMSO}$≈1.1.

cis-2N-DMSO (up)

cis-2N-DMSO (down)

trans-2N-DMSO (up)

trans-2N-DMSO (down)
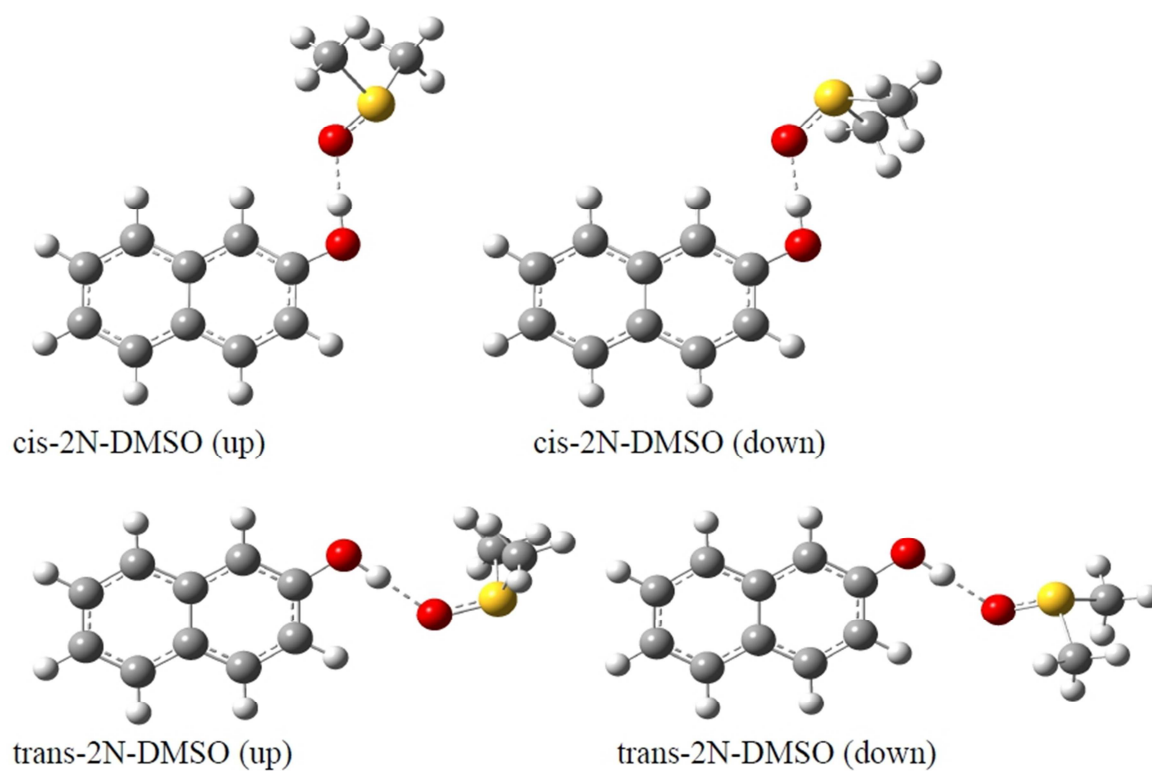
Figure S5: Isomers of the 2N-DMSO complex as obtained by TDDFT calculations.

cis-1N-DMSO (down)

trans-1N-DMSO (up)

trans-1N-DMSO (down)

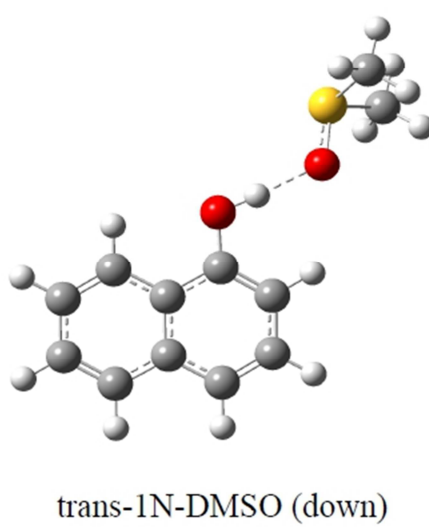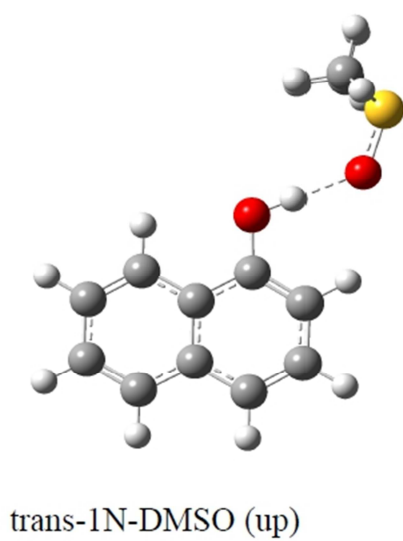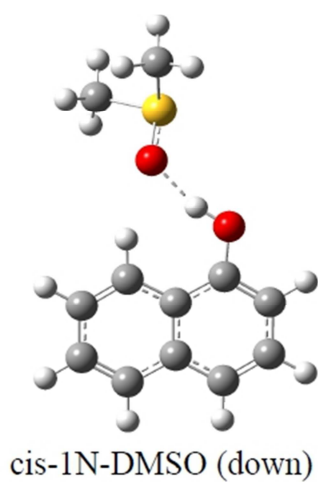**Figure S6:** Isomers of the 1N-DMSO complex as obtained by TDDFT calculations.

(I) S_0-state geometry

k	Isomers	Populations $f_{0,k}$	$S_0 \to {}^1L_a$ TDMs $\boldsymbol{\mu_{abs, k}}$ (arb. un.)		
			μ_x	μ_y	μ_z
1	*Cis-2N-DMSO (up)*	34.9	0.4333	0.0047	0.7188
2	*Cis-2N-DMSO (down)*	28.3	0.4319	-0.0029	0.7106
3	*Trans-2N-DMSO (up)*	16.8	0.4895	-0.0020	0.7379
4	*Trans-2N-DMSO (down)*	20.0	0.4919	0.0088	0.7503

(II) ^1L_a-state geometry

k	Isomers	Populations $f_{A,k}$	$^1L_a \to S_0$ TDMs $\boldsymbol{\mu_{a, k}}$ (arb. un.)		
			μ_x	μ_y	μ_z
1	*Cis-2N-DMSO (up)*	20.7	-0.4429	-0.0067	-0.8768
2	*Cis-2N-DMSO (down)*	13.5	-0.4398	0.0012	-0.8702
3	*Trans-2N-DMSO (up)*	26.3	0.5014	0.0008	0.8898
4	*Trans-2N-DMSO (down)*	39.5	-0.5061	-0.0139	-0.9011

(III) ^1L_b-state geometry

k	Isomers	Populations $f_{B,k}$	$^1L_b \to S_0$ TDMs $\boldsymbol{\mu_{b, k}}$ (arb. un.)		
			μ_x	μ_y	μ_z
1	*Cis-2N-DMSO (up)*	31.3	-0.2860	0.0001	0.3572
2	*Cis-2N-DMSO (down)*	23.8	0.4379	-0.0066	0.1327
3	*Trans-2N-DMSO (up)*	20.4	-0.2289	0.0001	0.3490
4	*Trans-2N-DMSO (down)*	24.5	-0.2384	-0.0019	0.3438

Table S1: Results of TDDFT calculations for the 2N-DMSO complex solved in DMSO. Leftmost three columns: isomer index, name, and populations estimated upon geometry optimization in the S_0 (panel I), ^1L_a (panel II) and ^1L_b (panel III) states. Next three columns: components of the absorption ($S_0 \to {}^1L_a$ transition, panel I), ^1L_a emission ($^1L_a \to S_0$ transition, panel II), and ^1L_b emission ($^1L_b \to S_0$ transition, panel III) TDMs, calculated for each isomer in the S_0, ^1L_a- and ^1L_b-state geometries respectively.

(I) S_0-state geometry

k	Isomers	Populations $f_{0,k}$ (%)	$S_0 \rightarrow {}^1L_a$ TDMs $\mathbf{\mu_{abs,k}}$ (arb. un.)		
			μ_x	μ_y	μ_z
1	*Cis-1N*	7	-0.0604	0.0000	0.9738
2	*Trans-1N*	93	-0.0898	0.0000	0.9939

(II) ^1L_a-state geometry

k	Isomers	Populations $f_{A,k}$ (%)	$^1L_a \rightarrow S_0$ TDMs $\mathbf{\mu_{a,k}}$ (arb. un.)		
			μ_x	μ_y	μ_z
1	*Cis-1N*	72	-0.0385	0.0349	1.0750
2	*Trans-1N*	28	-0.0680	0.0000	1.1225

(III) ^1L_b-state geometry

K	Isomers	Populations $f_{B,k}$ (%)	$^1L_b \rightarrow S_0$ TDMs $\mathbf{\mu_{b,k}}$ (arb. un.)		
			μ_x	μ_y	μ_z
1	*Cis-1N*	18	0.6782	-0.0001	0.0309
2	*Trans-1N*	82	-0.6999	0.0000	0.0095

Table S2: Results of TDDFT calculations for 1N solved in CHCl$_3$. Leftmost three columns: isomer index, name, and populations estimated upon geometry optimization in the S_0 (panel I), ^1L_a (panel II) and ^1L_b (panel III) states. Next three columns: components of the absorption ($S_0 \rightarrow {}^1L_a$ transition, panel I), ^1L_a emission ($^1L_a \rightarrow S_0$ transition, panel II), and ^1L_b emission ($^1L_b \rightarrow S_0$ transition, panel III) TDMs, calculated for each isomer in the S_0, ^1L_a- and ^1L_b-state geometries respectively.

(I) S_0-state geometry

k	Isomers	Populations $f_{0,k}$ (%)	$S_0 \rightarrow {}^1L_a$ TDMs $\mathbf{\mu_{abs,k}}$ (arb. un.)		
			μ_x	μ_y	μ_z
1	*Cis-1N-DMSO (down)*	0.0	-0.0586	0.0402	1.1045
2	*Trans-1N-DMSO (up)*	0.0	-0.1928	-0.0009	1.0447
3	*Trans-1N-DMSO (down)*	100.0	-0.1962	0.0096	1.0237

(II) ^1L_a-state geometry

k	Isomers	Populations $f_{A,k}$ (%)	$^1L_a \rightarrow S_0$ TDMs $\mathbf{\mu_{a,k}}$ (arb. un.)		
			μ_x	μ_y	μ_z
1	*Cis-1N-DMSO (down)*	1.6	0.0299	-0.0542	-1.2089
2	*Trans-1N-DMSO (up)*	42.1	0.1821	0.0128	-1.1498
3	*Trans-1N-DMSO (down)*	56.3	-0.1948	0.0315	1.1235

(III) ^1L_b-state geometry

k	Isomers	Populations $f_{B,k}$ (%)	$^1L_b \rightarrow S_0$ TDMs $\mathbf{\mu_{b,k}}$ (arb. un.)		
			μ_x	μ_y	μ_z
1	*Cis-1N-DMSO (down)*	0.0	0.8505	0.0050	0.0299
2	*Trans-1N-DMSO (up)*	0.0	-0.8570	0.0101	0.0149
3	*Trans-1N-DMSO (down)*	100.0	-0.9155	-0.0122	0.0242

Table S3: Results of TDDFT calculations for the 1N-DMSO complex solved in DMSO. Leftmost three columns: isomer index, name, and populations estimated upon geometry optimization in the S_0 (panel I), ^1L_a (panel II) and ^1L_b (panel III) states. Next three columns: components of the absorption ($S_0 \rightarrow {}^1L_a$ transition, panel I), ^1L_a emission ($^1L_a \rightarrow S_0$ transition, panel II), and ^1L_b emission ($^1L_b \rightarrow S_0$ transition, panel III) TDMs, calculated for each isomer in the S_0, ^1L_a- and ^1L_b-state geometries respectively.

	1N-DMSO	2N-DMSO	1N in $CHCl_3$
r_A (φ_A)	0.399 (2.2)	0.397 (3.9°)	0.398 (3.1°)
r_B (φ_B)	-0.172 (77.6°)	-0.054 (60.4°)	-0.195 (84.6°)

Table S4: Characteristic values of anisotropy predicted by TDDFT for 1N-DMSO in DMSO solution, 2N-DMSO in DMSO solution and 1N in $CHCl_3$ solution emitting from the ^1L_a and ^1L_b states after initial excitation to the ^1L_a state. r_A and r_B can be equivalently expressed as characteristic "effective" absorption-emission angles φ_A and φ_B, as defined by the relation $r_{A,B} = 0.2 \, (3\cos^2 \varphi_{A,B} - 1)$.